Journal of Magnetic Resonance 247 (2014) 22–30

Contents lists available at ScienceDirect

Journal of Magnetic Resonance

journal homepage: www.elsevier.com/locate/jmr

A miniaturized NQR spectrometer for a multi-channel NQR-based detection device

Samo Beguš [a], Vojko Jazbinšek [b], Janez Pirnat [b], Zvonko Trontelj [b,*]

[a] University of Ljubljana, Faculty of Electrical Engineering, Ljubljana, Slovenia
[b] Institute of Mathematics, Physics and Mechanics, University of Ljubljana, Ljubljana, Slovenia

ARTICLE INFO

Article history:
Received 12 June 2014
Revised 1 August 2014
Available online 14 August 2014

Keywords:
Nuclear quadrupole resonance
Portable spectrometer
Software defined radio platform
Illicit substances detection
LabView Virtual instrument

ABSTRACT

A low frequency (0.5–5 MHz) battery operated sensitive pulsed NQR spectrometer with a transmitter power up to 5 W and a total mass of about 3 kg aimed at detecting ^{14}N NQR signals, predominantly of illicit materials, was designed and assembled. This spectrometer uses a standard software defined radio (SDR) platform for the data acquisition unit. Signal processing is done with the LabView Virtual instrument on a personal computer. We successfully tested the spectrometer by measuring ^{14}N NQR signals from aminotetrazole monohydrate (ATMH), potassium nitrate (PN), paracetamol (PCM) and trinitrotoluene (TNT). Such a spectrometer is a feasible component of a portable single or multichannel ^{14}N NQR based detection device.

© 2014 Elsevier Inc. All rights reserved.

1. Introduction

Nuclear quadrupole resonance (NQR), a younger sister of nuclear magnetic resonance (NMR), is a non-invasive radiofrequency (RF) spectroscopic method. The Hamiltonian is based on the electric interaction between nuclei with nonzero electric quadrupole moment and the internal electric field gradient created by the surrounding electrons whose distribution is determined by the crystal structure of the solid material: $\mathcal{H} = \underline{Q} \cdot \underline{\nabla E}$, where $\underline{Q}$ is the tensor of electric quadrupole moment describing the charge distribution in the nucleus and $\underline{\nabla E}$ is the tensor of electric field gradient at the nucleus. ^{14}N nuclei have spin $I = 1$ and nonzero electric quadrupole moment. Since nitrogen is present in a large number of organic and inorganic compounds, ^{14}N NQR can be very effective in studying their structure, polymorphism and structural dynamics, as well as in detecting the presence of nitrogen-containing illicit materials like narcotics, explosives (improvised, the residues of explosives after the ceased armed actions or attacks) and counterfeit medicines [1–4]. The detection of the mentioned illicit materials in particular caused a renaissance in NQR RF spectroscopy and its applications, together with several improvements in the signal-to-noise (S/N) ratio in the last 10 years or so. That was necessary mainly owing to the fact that in these cases low frequency nitrogen NQR (^{14}N NQR) is almost exclusively detected. For ^{14}N with spin $I = 1$, the NQR energy levels and allowed transitions between them are shown in Fig. 1. The corresponding frequencies are equal to [5,6]:

$$\nu^+ = \frac{e^2qQ}{4h}(3+\eta), \quad \nu^- = \frac{e^2qQ}{4h}(3-\eta) \quad \text{and} \quad \nu^0 = \frac{e^2qQ}{2h}\eta \qquad (1)$$

Here, $e^2qQ/h = Q_{cc}$ is the quadrupole coupling constant where eQ is the nuclear electric quadrupole moment, $eq = q_{zz}$ is the maximal component of the electric field gradient tensor, e is the unit charge, h the Planck constant, and $\eta = (q_{xx} - q_{yy})/q$ is the asymmetry parameter.

When using a ^{14}N NQR spectrometer in the detection device for illicit materials, we are often faced with the requirement for a geometrically small device which can be adapted for particular detection purposes, sometimes in a multi-NQR frequency, ie a multichannel configuration. Another need for a small NQR spectrometer is in the on-line monitoring of possible appearance of polymorphism in the chemical industry, mainly in the production of medicines.

The aim of this work was thus to design and build a low frequency (0.5–5 MHz) battery operated highly sensitive pulsed NQR spectrometer with a transmitter power of up to 5 W and a total mass of about 3 kg or less. Due to low power the pulse sequences will be longer in comparison to an equivalent classical laboratory NQR spectrometer, in particular, the $\pi/2$ pulse is longer, the excitation bandwidth is narrower and we have to consider that the sample volume, which is irradiated with the magnetic part of RF, is smaller.

* Corresponding author.
E-mail address: zvonko.trontelj@fmf.uni-lj.si (Z. Trontelj).
URL: http://fizika.imfm.si (Z. Trontelj).

http://dx.doi.org/10.1016/j.jmr.2014.08.002
1090-7807/© 2014 Elsevier Inc. All rights reserved.

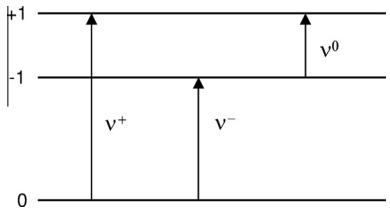

Fig. 1. Quadrupole energy levels and allowed transitions for the spin 1 nucleus.

The miniaturization of RF spectrometers is today theoretically and practically a feasible project [7–9]. We used a field-programmable gate array (FPGA) and software in the form of LabView Virtual instruments. The resulting low frequency and low power miniaturized NQR spectrometer was tested by measuring ^{14}N NQR signals from samples of aminotetrazole monohydrate (ATMH) – $CH_3N_5 \cdot H_2O$, potassium nitrate (PN) – KNO_3, paracetamol (PCM) – $C_8H_9NO_2$ and trinitrotoluene (TNT) – $C_7H_5O_6N_3$.

2. Experimental

2.1. The concept of a miniaturized NQR spectrometer

Fig. 2 shows the block scheme of the miniaturized NQR spectrometer. Since we expected a maximal power of 5 W to be sufficient, all electronic elements were small and we mounted them in the form of a close packed hybrid structure. The front end of the miniaturized NQR spectrometer was a standard one with a tank circuit and matching circuit as it will be described in details in Section 2.2. The preamplifier, signal amplifier and power amplifier were chosen to obtain a miniaturized yet still functional NQR spectrometer. The software defined radio platform N200, from Ettus Research™ [10] was used for data acquisition and signal generation. The platform includes a dual, 14 bit, 100 mega samples per second (MSPS) analogue-to-digital converter (ADC) and dual, 16 bit, 400 MSPS digital-to-analogue converter (DAC), FPGA, as well as a 1 Gbit Ethernet interface.

2.2. Tank circuit, matching circuit and planar coils

Tank circuit was realized in two forms (i) with a standard solenoidal coil: length l = 8 cm, diameter d = 12 mm and (ii) with a planar (2D) coil: inner radius r_1 = 1 cm and outer radius r_2 = 6 cm and a variable high voltage capacitor for frequency tuning. Two planar coils can be combined in a gradiometer configuration. In the case of planar coil configuration the coil is placed close to the measured

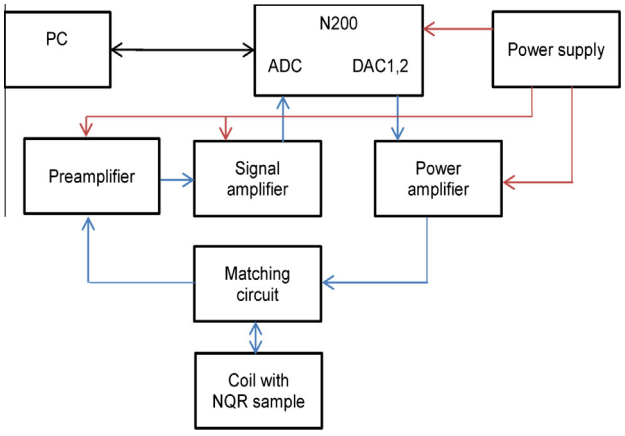

Fig. 2. Block scheme of miniaturized NQR spectrometer for ^{14}N NQR detection.

object, for instance near a box of suspicious - counterfeit medicine. The planar coil design was based on an Archimedean spiral described in polar coordinates as

$$r(\varphi) = \frac{a}{2\pi}\varphi + r_1, \quad \vec{r} = r(\varphi)\begin{pmatrix}\cos\varphi \\ \sin\varphi\end{pmatrix}, \tag{2}$$

where parameter a represents a constant radius increment in one turn when the polar angle φ is increased by 2π. Higher constancy of the magnetic field magnitude near the coil plane was searched for with a modified Archimedean spiral

$$r(\varphi) = \left(\frac{a}{2\pi}\varphi\right)^p + r_1, \tag{3}$$

where the exponent p provides either an increase of space between turns ($p > 1$) or its decrease ($p < 1$) when increasing the polar angle φ. Magnetic field at the site $\vec{r}'$ for a constant current I along the spiral was calculated with a numerical integration of Biot–Savart law

$$\vec{H}(\vec{r}') = \frac{I}{4\pi}\sum_{\varphi=\varphi_0}^{\varphi_0+2\pi n}\frac{\vec{t}\times(\vec{r}'-\vec{r})}{|\vec{r}'-\vec{r}|^3}\Delta\varphi, \tag{4}$$

where $\vec{r}$ is defined in (2) or (3), $\vec{t} = \frac{\partial\vec{r}}{\partial\varphi}$ is a tangent on the spiral curve (direction of the current element $I\vec{t}\Delta\varphi$) and n is a number of coil turns. Fig. 3(a) and (b) displays geometry of the Archimedean coil with a n = 16 turns and the modified coil with a $p = 0.1$. Fig. 4(a) and (b) shows corresponding calculated magnetic field above the coil, respectively.

The induced NQR signal amplitudes are very small and therefore high amplification of the detected signal is needed. That was achieved by using two amplifiers: a preamplifier and a signal amplifier. Several preamplifiers were tested (Miteq AU-1579 low noise 50 Ω preamplifier, Hi-Z low noise preamplifier HVA-200M-40-F and a BF998 Hi-Z custom-built preamplifier).

Two impedance matching and duplexer circuit were used. A configuration with a high-impedance preamplifier (Fig. 5(a)) and one with a low-input impedance preamplifier (Fig. 5(b)).

Only minor differences in performance were observed.

2.3. Signal amplifiers

As a signal amplifier we constructed a two stage circuit. The 1st stage was the Norton Noiseless Feedback Amplifier [11] with appropriate input protection against high voltage pulses, while the 2nd stage was a wide bandwidth current feedback operational amplifier (Figs. 6 and 8(a)). The output stage of the signal amplifier was designed to limit its output voltage to safe values for the data acquisition board.

2.4. Power amplifier

A home built wide bandwidth power amplifier was based on the operational amplifier LT1210.

The LT1210 needs only an output impedance matching circuit and a simple interface for switching between normal operation and the disabled state. It has in-built thermal protection and short-circuit protection, which add to the ruggedness of the amplifier, especially when operating with non-optimally matched loads. The circuit is shown in Fig. 7. Considering that we use at most only about 3% of measuring time as an active RF radiation time we can safely apply the linear power amplifier architecture. The efficiency of the power amplifier (P_{out}/P_{in}) used is up to 26%, depending on operating conditions.

The power amplifier was built inside the N200 case owing to its small size and is marked by a rectangle in Fig. 8(b).

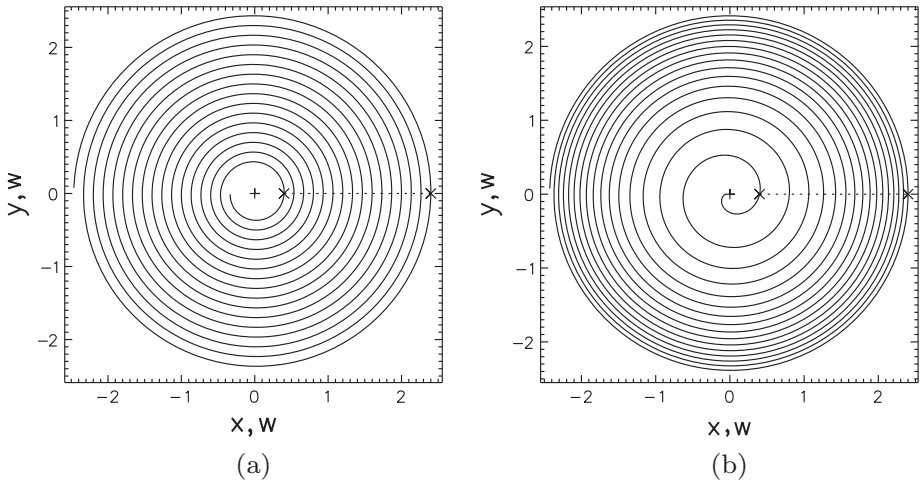

Fig. 3. Geometry of coils (a) the Archimedean coil with a $n = 16$ turns and (b) the modified coil with a $p = 0.1$. Coordinates are in units of the coil half width $w = (r_2 - r_1)/2 = 2.5$ cm, where $r_1 = 1$ cm is the inner radius and $r_2 = 6$ cm is the outer radius. The coil started with the polar angle $\varphi_0 = -\pi$, while r_1, r_2 (marked with $\times$) and $2w$ (dashed line) are defined with the polar angle $\varphi = 0$.

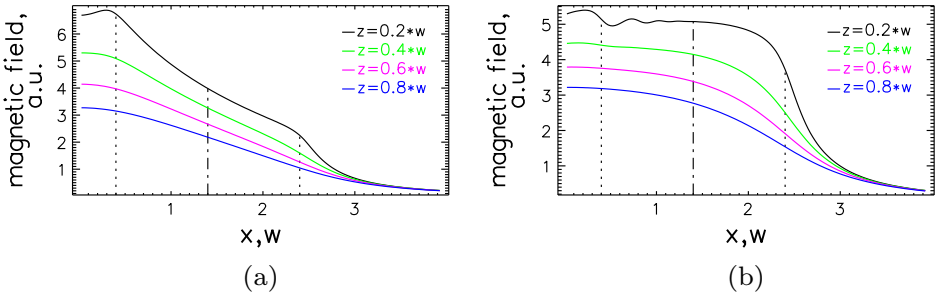

Fig. 4. Magnetic field magnitude above (a) the Archimedean coil and (b) the modified coil with $p = 0.1$ from Fig. 3. Magnetic field is calculated at different distances z measured in units of the coil half width $w = 2.5$ cm. Dashed vertical lines denote the inner (r_1) and the outer (r_0), and the dashed-dot line the mean coil radius.

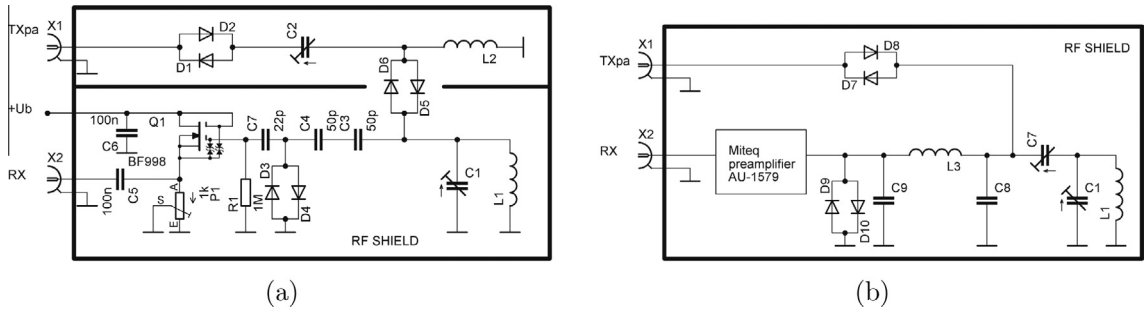

Fig. 5. Matching, preamplifier and duplexer circuit. L1 is the sample-coil. The C2–L2 resonant circuit is used for voltage step-up transformation to efficiently couple RF energy to the sample coil L1 via coupling diodes D5 and D6. The C8–L3–C9 circuit is a lumped-element equivalent of the quarter wavelength cable used for duplexer, capacitor C7 is used for impedance matching.

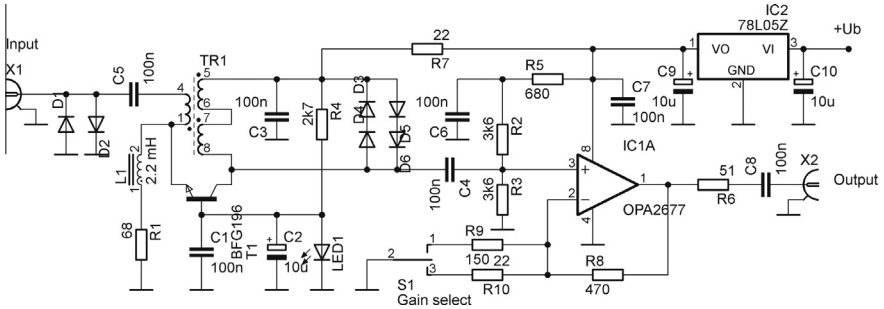

Fig. 6. Signal amplifier with Norton Noiseless stage and wide bandwidth current feedback operational amplifier.

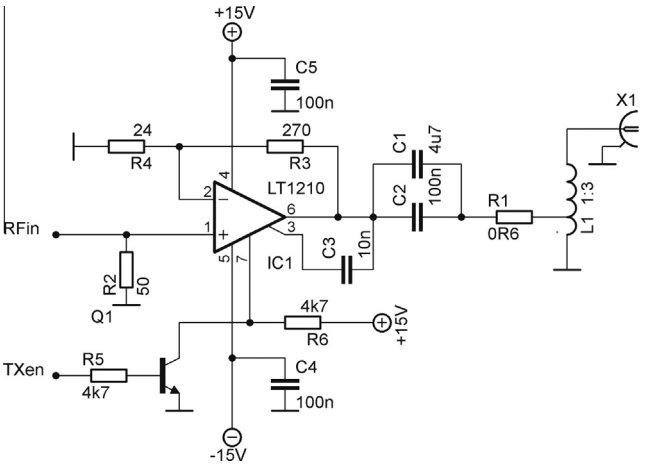

Fig. 7. Wide bandwidth power amplifier with LT1210 current feedback amplifier.

2.5. Data acquisition – applied software

LabView Virtual instruments [12] were used for all pulse NQR parameters preparation and for the consequent data processing. Data export is possible in plain ASCII format for maximum compatibility. All saved data can also be processed off-line.

The program flow for the miniaturized NQR spectrometer is shown in Fig. 9. The parameters used in the NQR pulse sequence are first chosen. They are optimized later if the function *optimization* is selected, otherwise the NQR pulse sequence and received reference signal(s) are generated according to the chosen parameters. The first DAC of the N200 is used for transmitter signal generation. The second DAC is used for generating the signal for disabling the power amplifier during the receiving sequences. Thus there is no need for FPGA software modification.

The phase of each π pulse can be set in two different ways:

- The same phase for each π pulse ("copy-paste" procedure). Receiver reference signals ("local oscillator" in-phase and quadrature signals) for RF mixing have the same starting phase for each received pulse. For best performance the function *optimization* of the spectrometer parameters should be turned on. With optimization the frequency of the transmitted signal is fine-tuned and the length of the transmitting $\pi/2$ pulse, π pulse and time used for receiving are adjusted in such a way that an integer number of periods is transmitted in each part of the transmitting sequence.
- The π pulses are derived from the generated continuous phase sine wave via a function which is active only during the π pulse. Because the NQR signal frequency received could be different from the transmitting excitation RF frequency, the receiver

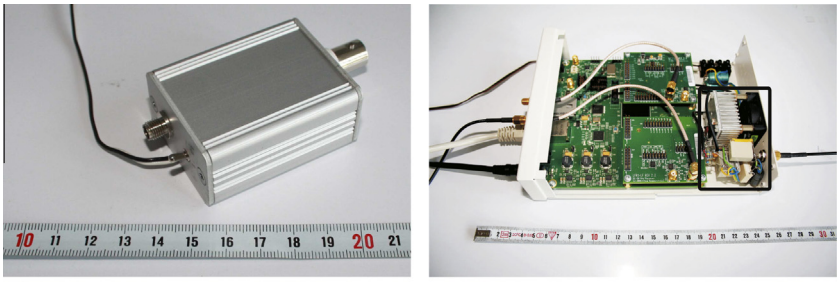

Fig. 8. Two stage signal amplifier (a) and power amplifier built in the N200 case (b), with measuring tape in cm.

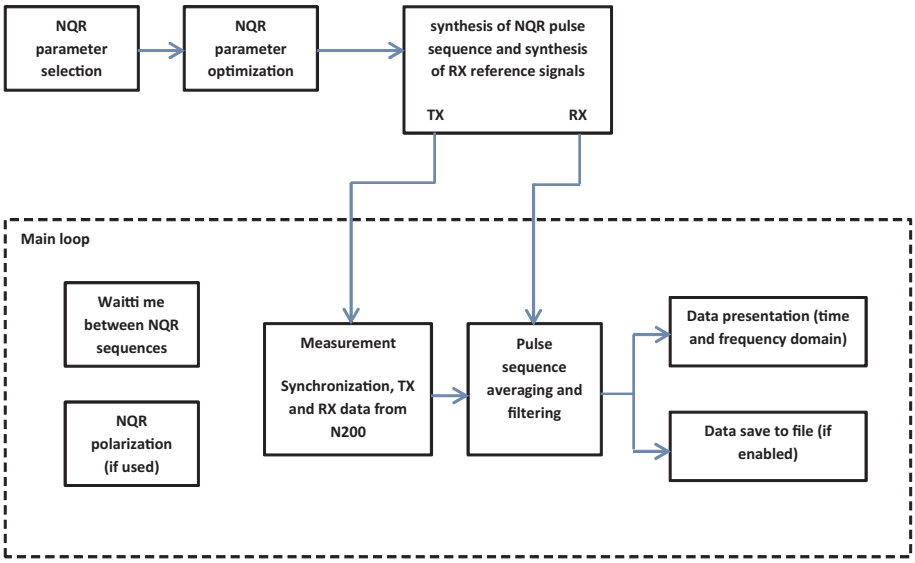

Fig. 9. Program flow in the miniaturized NQR spectrometer.

reference signals ("local oscillator" in-phase and quadrature signals) for the RF mixing are calculated to have zero phase just at the center between two π pulses (NQR echo center).

We applied predominately the first ("copy-paste") procedure. In the main loop (Fig. 9) the previously prepared pulse sequence is transmitted and the NQR signal received. When using polarization enhancement [3], the appropriate auxiliary control signals are generated. The signals received are averaged to improve the *S*/*N* ratio. The averaged received signal is filtered by a low-pass and a high-pass filter with adjustable filter order and corner frequencies to enhance the displayed signal in the time domain. Irrespective of the setting of the displayed signal, all the data are saved in an unfiltered state. Due to high sampling frequency (up to 20 MHz) the saved signals are filtered (low-pass filter with a corner frequency of 250 kHz) and resampled at 1 MHz sampling frequency so that the usable signal bandwidth is limited to ±250 kHz of the received frequency, combining in-phase and quadrature signals.

The number of pulses in the sequence used for averaging can be chosen arbitrarily.

The phase cycling can be turned on to suppress the ringing effect. Here, the π pulse phase of every second sequence iteration is inverted, thus producing ringing with the opposite phase which can be suppressed by averaging.

In both, data acquisition and data analysis, we gain from the user friendly program steps which are part of the LabView application. All modifications which are necessary, when different samples are measured, can be introduced transparently and quickly.

2.6. Measurement of the performance of the miniaturized NQR spectrometer

We checked the performance of the miniaturized NQR spectrometer by measuring the ^{14}N NQR signals of the characteristic compounds ATMH [13], PN [14], PCM [28] and TNT [3], studied previously by a classical pulse NQR spectrometer. In all cases the volumes of typical samples (with specific density approx. 1 g/ccm) were less than 10 ccm. That means we used for these small sample volumes (ATMH, PN, TNT and PCM) a cylindrical solenoid coil: length 8 cm, diameter 1.2 cm. In addition, we also made a test with the planar coil: inner diameter 2 cm, outer diameter 12 cm, equidistant spacing between turns. Generally, the planar coil requires larger amount of tested material (Fig. 14).

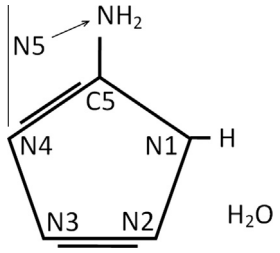

Fig. 10. Aminotetrazole monohydrate (ATMH).

2.6.1. ^{14}N NQR in aminotetrazole monohydrate

The tetrazole ring CH_2N_4 (TZ) appears in a number of new pharmaceutical products as a functional group [15–18]. TZ can also act as a starting point for new explosives [19–21], for anti-corrosive coatings [22], for information recording systems [23], and in many synthetic pathways as the precursor of various nitrogen-containing heterocycles. Investigation of tetrazole compounds is relevant to studies of the application of ^{14}N NQR for the detection of explosives, as well as the study of polymorphism in some pharmaceuticals [24].

Determination of ^{14}N frequency and optimized ^{14}N NQR parameters for the ν_0 line of nitrogen atom number 5 in ATMH (Fig. 10) in the temporal and frequency domain with the miniaturized NQR spectrometer are shown in Fig. 11(a) and (b). As expected the $\pi/2$ pulse is longer (125 μs) in comparison to our earlier measurements (30 μs) on a classical pulse NQR spectrometer [13]. However, we were still able to position 20 π pulses in the modified Carr–Purcell (CP) sequence and obtained a very good *S*/*N* ratio for this low frequency line. In the experiment [13] 30 π pulses were included in the modified Carr–Purcell (CP) sequence.

In Fig. 12 the LabView Virtual instrument is shown used for reading and post-processing the saved data. The central frequency can be changed and corner frequencies, filter order and time frame of the displayed data can be set. The number of averaged echoes in one sequence can be set arbitrarily.

2.6.2. ^{14}N NQR in potassium nitrate

KNO_3 belongs to the class of nitrates which are often applied for improvised explosive devices. The molecule of PN contains one nitrogen atom and one potassium atom. Therefore both, ^{14}N NQR and ^{39}K NQR can be used to detect the presence of PN. At room temperature we observed one ^{39}K NQR line at 666.4 kHz and one set of ^{14}N NQR lines (567 kHz and 559 kHz for the ν^+ and ν^- transition frequencies) which indicates the equivalence of all nitrogen positions in the crystal lattice. Potassium nitrate has an orthorhombic crystal structure at room temperature, which transforms

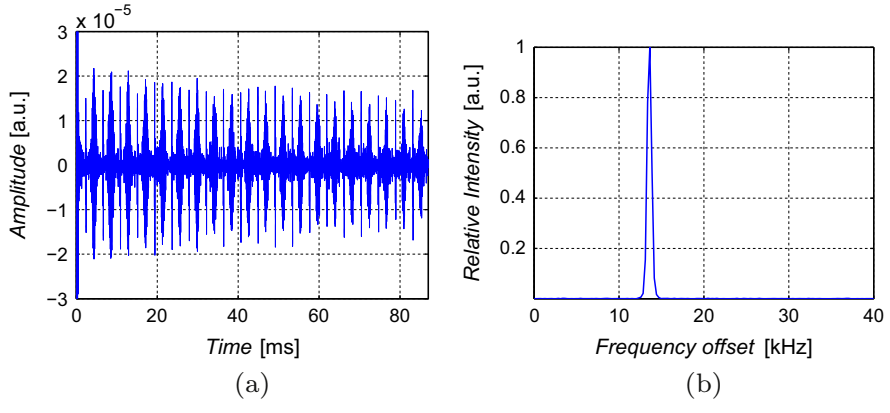

Fig. 11. Aminotetrazole monohydrate sample ^{14}N NQR signal after 1000 averaged pulse sequences with 20 pulses (panel a) in each sequence. A whole sequence of 20 pulses is shown. The signal bandwidth is 5 kHz, 2nd order Butterworth band-pass filter. The peak in the frequency domain plot is at 1213.6 kHz (panel b). The frequency zero value is equal to 1200 kHz.

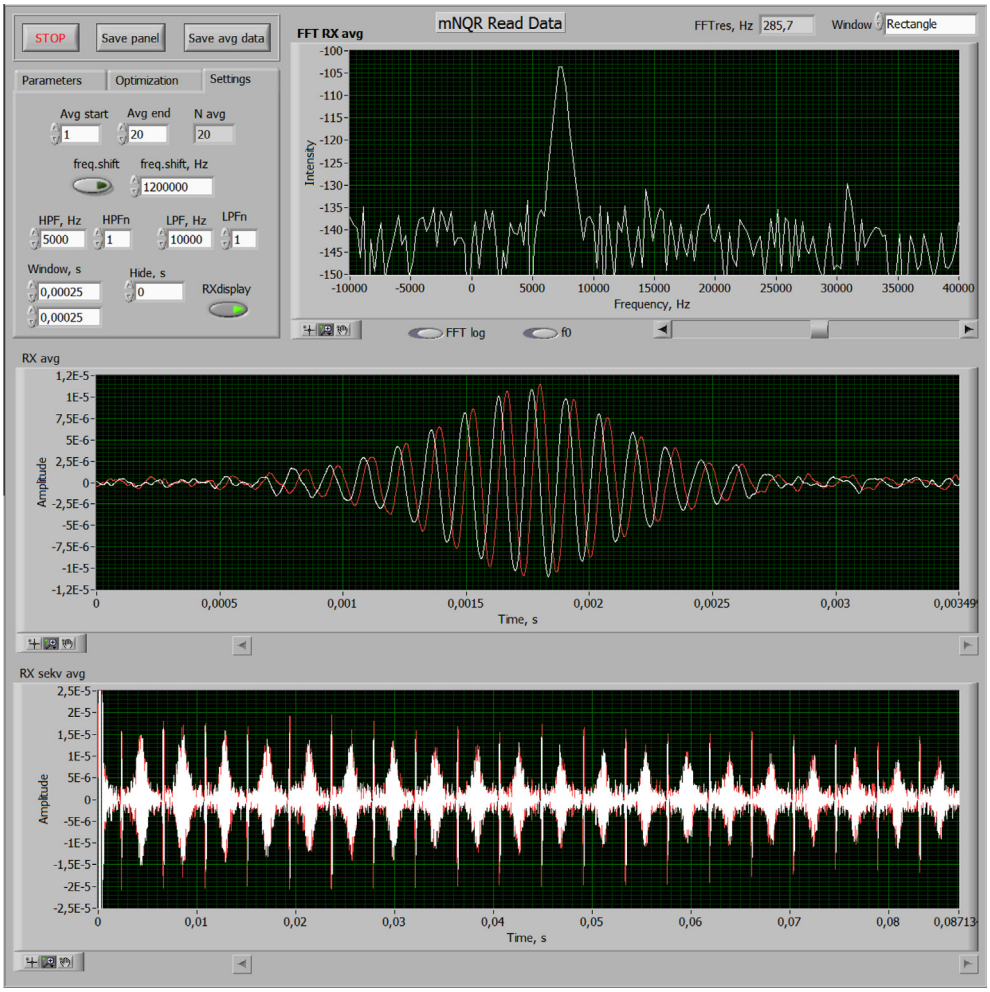

Fig. 12. LabView control panel of the Virtual instrument front panel used for reading and post-processing of saved data. Upper panel: ^{14}N NQR FFT spectrum, middle panel real and imaginary signal components in temporal domain, lower panel: averaged received signal with the chosen pulse sequence. Spectrometer settings are shown in Table 1. ATZMH data is shown.

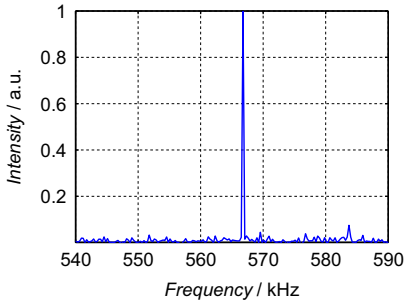

Fig. 13. ^{14}N NQR frequency spectrum of potassium nitrate sample, obtained after 100 averaged pulse sequences with 10 pulses in each sequence. The peak in the frequency domain plot is at 566.5 kHz.

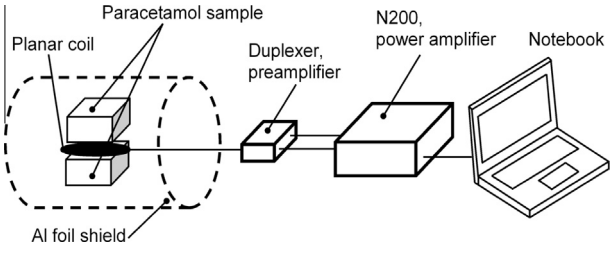

Fig. 14. Schematic of the paracetamol measurement set-up with a battery powered miniaturized ^{14}N NQR spectrometer combined with a planar coil. The sample in this experiment consisted of 2 × 6 parcels, each with 20 analgesic pills in two parallel plains with a planar coil between them. A modest shielding with a household Al foil was applied.

to a trigonal structure at 129 C. The *S*/*N* ratio is rather poor and we needed to apply signal averaging. The frequency spectrum of the ν^+ ^{14}N NQR line is shown in Fig. 13. The $\pi/2$ length was 125 μs while with classical pulse NQR spectrometer it was 30 μs.

2.6.3. ^{14}N NQR in paracetamol

To test the ability of this low power NQR spectrometer to detect possible counterfeit medicines, the ^{14}N NQR detection of the PCM [28] was carried out by using the planar sample coil. As a standard in these tests different analgesic pills with active pharmaceutical ingredient paracetamol were used. In a large paper box with smaller packets of analgesics the planar RF coil was inserted. We were able to detect the ^{14}N NQR signal even with the presence of metal foil on one side of blister packing of different analgesics containing paracetamol. The impedance matching was achieved by matching circuit with low input impedance preamplifier shown in Fig. 5(b). This experiment was carried out in a partially shielded environment (thin aluminum foil placed around the sample and planar sensing coil). The sample pills in blister packaging were placed on top and below a flat planar coil, see Fig. 14. Results are shown in Fig. 15.

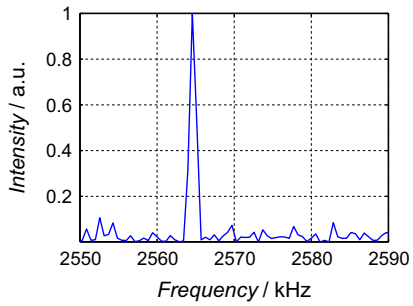

Fig. 15. ^{14}N NQR frequency spectrum of paracetamol, obtained after 20 averaged pulse sequences with 100 pulses in each sequence.

2.6.4. ^{14}N NQR in trinitrotoluene

^{14}N NQR detection of the well known and broadly applied explosive TNT still presents a challenge. The reason is in the weak quadrupole coupling of nitrogen in the NO_2 groups and consequently the low ^{14}N NQR transition frequencies with a very low S/N ratio of the ^{14}N NQR signals. With two crystallographically inequivalent molecules in the unit cell we expect 6 ν^+ and 6 ν^- lines (3 in-equivalent nitrogen nuclei in a molecule).

In addition, TNT appears in two different crystallographic modifications, orthorhombic and monoclinic [4]. Hence we have two different NQR spectra, each consisting of 6 lines for the ν^+ and 6 for the ν^- ^{14}N NQR transition frequencies. The existence of two different crystallographic modifications makes the detection of TNT difficult as it is not known in advance which modification is prevalent. This problem can be successfully solved because the different polymorphic forms of TNT have different ^{14}N NQR resonance lines, as expected [4]. Namely, the ^{14}N nuclei in the different polymorphs exhibit different electric field gradients at their positions in the crystal structure. This fact enabled us to determine the crystal modification of the measured TNT sample. Fig. 16(a) and (b) present the ^{14}N NQR ν^+ frequency spectra of monoclinic and orthorhombic TNT samples. The lower frequency resolution of the miniaturized ^{14}N NQR spectrometer is clearly evident in the closely lying ^{14}N NQR lines at 844.3 kHz and 842.8 kHz for monoclinic TNT, denoted by A in Fig. 16(a), which cannot be resolved with this spectrometer. The same is true for the closely lying ^{14}N NQR lines at 846.8 kHz and 848.3 kHz for orthorhombic TNT, denoted by B (Fig. 16(b)). We only can see that the unresolved NQR lines in monoclinic and orthorhombic TNT are broader and the line B in the Fig. 16(b) has an additional shoulder. For comparison see Fig. 17 obtained with a classical NQR spectrometer, where the corresponding NQR lines A1 and B1 are resolved. The frequency resolution Δf is determined by the acquisition time – T or equivalently by the number of samples N and sampling frequency – f_s ($\Delta f = f_s/N = 1/T$). These parameters were chosen according to the detected material properties and the requirement to get the best S/N ratio. In our case we have for the ATMH $T = 4.00\ \text{ms} - 0.25\ \text{ms} = 3.750\ \text{ms}$; $1/T = 0.27$ kHz and for the TNT

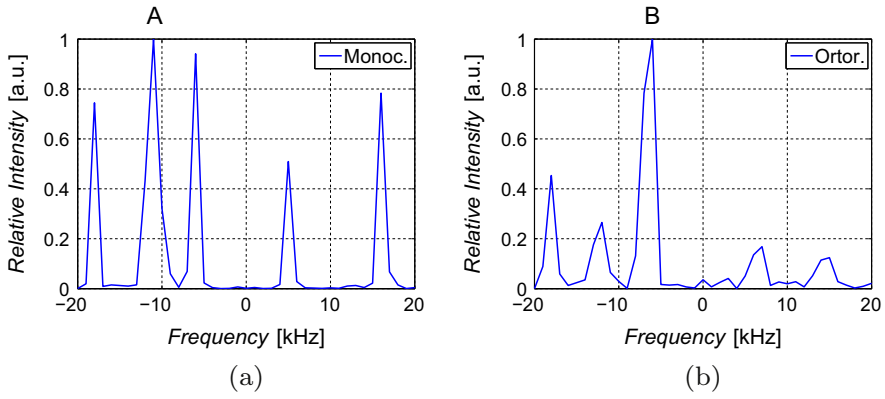

Fig. 16. ^{14}N NQR spectra of monoclinic phase (a) and orthorhombic phase (b) of TNT obtained with the miniaturized NQR spectrometer. The frequency zero is equal to 855 kHz.

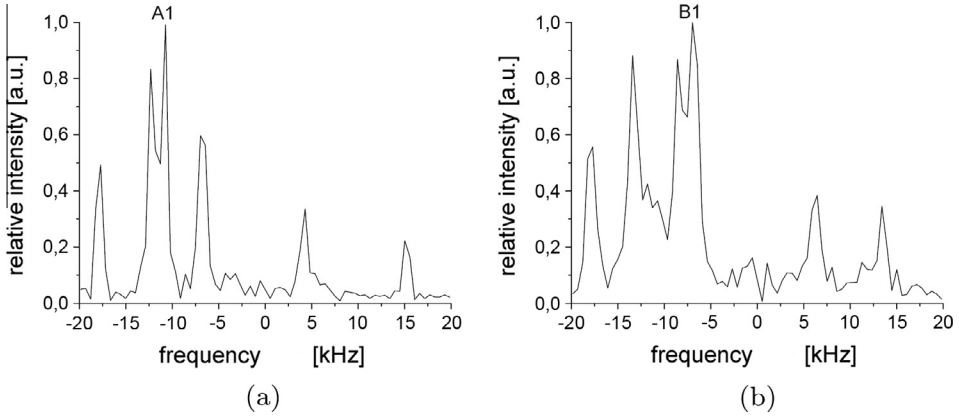

Fig. 17. ^{14}N NQR spectra of monoclinic phase (a) and orthorhombic phase (b) of TNT obtained with a classical 500 W pulsed NQR spectrometer, working with 60 W. The frequency zero is equal to 855 kHz.

Table 1
Settings used with miniaturized NQR spectrometer and a classical high-power (HiPwr) pulsed NQR spectrometer (for TNT only).

	k	n	t_0 [s]	t_m [min]	f_{rx} [kHz]	f_{tx} [kHz]	P_{tx} [W]	$t_{\pi/2}$ [ms]	t_{rx} [ms]	f_r [kHz]
ATZMH	1000	20	3	50	1206	1213.5	1	0.125	4.00	0.27
KNO_3	100	10	15	25	564	567.0	1	0.175	4.00	0.27
PCM	20	100	15	5	2560	2564.0	2	0.400	2.00	0.57
•TNT	16	10	30	8.4	840	837.0	3	0.125	1.25	1.00
	16	10	30	8.4	840	843.0	3	0.125	1.25	1.00
	16	10	30	8.4	840	847.5	3	0.125	1.25	1.00
	16	10	30	8.4	840	860.0	3	0.125	1.25	1.00
	16	10	30	8.4	840	869.5	3	0.125	1.25	1.00
$•TNT_{HiPwr}$	10	15	30	5	845	845.0	60	0.03	2.048	0.6
	10	15	30	5	845	865.0	60	0.03	2.048	0.6

k – number of sequence iterations; n – number of π pulses; t_0 – time between iterations; t_m – measurement time; f_{rx} – receiver local oscillator frequency; • – polarization enhancement used; f_{tx} – transmitter frequency; P_{tx} – transmitter output power; $t_{\pi/2}$ – $\pi/2$ pulse duration; t_{rx} – receiving time; f_r – FFT spectrum frequency resolution.

Table 2
Optimized settings used with miniaturized NQR spectrometer.

	f_{rx} [kHz]	$t_{\pi/2}$ [ms]	$t_{\pi/2o}$ [ms]	f_{tx} [kHz]	f_{txo} [kHz]	t_{rx} [ms]	t_{rxo} [ms]
ATZMH	1206	0.125	0.12525	1213.5	1213.5888	4.00	3.99970
KNO_3	564	0.175	0.17637	567.0	567.0000	4.00	4.00000
PCM	2560	0.400	0.40010	2564.0	2564.1208	2.00	1.99990
TNT	840	0.125	0.12665	837.0	836.8035	1.25	1.25000
	840	0.125	0.12575	843.0	842.8992	1.25	1.25045
	840	0.125	0.12510	847.5	847.4296	1.25	1.25085
	840	0.125	0.12550	860.0	860.5852	1.25	1.25030
	840	0.125	0.12650	869.5	869.5652	1.25	1.25120

f_{rx} – receiver local oscillator frequency; $t_{\pi/2}$ – $\pi/2$ pulse duration; $t_{\pi/2o}$ – optimized $\pi/2$ pulse duration; f_{tx} – transmitter frequency; f_{txo} – optimized transmitter frequency; t_{rx} – receiving time; t_{rxo} – optimized receiving time.

sample T = 1.25 ms − 0.25 ms = 1.00 ms; $1/T$ = 1 kHz. We have considered the removal of transients after the π pulse by subtracting approximately 0.25 ms.

Table 1 shows the settings used with the miniaturized NQR spectrometer and the classical 500 W – however, working here with 60 W – pulsed NQR spectrometer (for TNT only). Polarization enhancement for TNT samples mentioned in Section 2.5 and in Table 1 was performed with the permanent FeNdB magnet [29]. The polarization time for protons was about 15 s, magnetic field at the center of the sample was about 300 mT, the demagnetization time was between 300 ms and 500 ms and the measured signal intensity enhancement factor for the ν^+ line at 870 kHz in monoclinic TNT was about 10. Detail of polarization enhancement device, which we applied, is in [3,29]. Table 2 shows the optimized settings used with the miniaturized NQR spectrometer. The transmitter frequencies used were the same for both crystallographic modifications.

3. Discussion and conclusions

NQR spectroscopy was demonstrated already in the middle of previous century to be able to detect the nitrogen (^{14}N) nuclear quadrupole resonance, [5]. Practically all ^{14}N NQR lines are below 5 MHz and therefore it was difficult (in the past) to achieve in reasonably short measuring time a high enough S/N ratio for any practical application, like the detection of nitrogen-containing illicit materials. In the last ten or fifteen years, some new approaches appeared [2,3,25–27] and the S/N ratio was improved to the extent that presently we can contactless detect the most important illicit materials reasonably rapidly in a laboratory environment.

Today's requirements are directed towards a low power ^{14}N NQR spectrometer that may lead to a portable multi-channel NQR device which would be able to rapidly detect several illicit materials. We showed in this work that such a type of ^{14}N NQR spectrometer functions well in all cases where the ^{14}N NQR line parameters (line width, T_2, T_1) also allow a longer duration of π pulses. This miniaturized ^{14}N NQR spectrometer was constructed with commercially available microelectronic components. It is a single channel pulsed ^{14}N NQR spectrometer of around 2 kg mass (without the battery) and operates with a maximal RF power of 5 W. A note-book PC is needed for communication with the spectrometer and for data acquisition and analysis.

We tested the usual notebook Li-ion rechargeable battery of 0.33 kg and 55 W h capacity. With this battery the miniaturized NQR spectrometer can operate for about 4 h. As a test of a battery operated miniaturized NQR spectrometer, equipped with the planar coil, a measurement of genuine paracetamol sample, Fig. 15, was taken in the main parcel sorting building at the airport. All other samples, discussed in this article were taken in the laboratory and the measuring system was mains powered. Li-ion rechargeable battery we used has approximately equal operation time as a notebook in the battery powered mode. A modest shielding in form of a thin aluminum foil metal cylinder or a metal mesh with about 1 mm opening helps when electromagnetic disturbances are present. Gradiometric configuration of the pick-up coil was also tested and improvement in signal to noise ratio was obtained.

In conclusion, we were able to detect all the usually met explosives (including trinitrotoluene – TNT – with polarization enhancement) and improvised explosives in reasonable measuring times. A multi-channel detection device, based on the detection of ^{14}N NQR seems to be a feasible project.

Acknowledgments

This research was partly funded by the Slovenian Research Programs P2-0348, P2-0250 and by the EC FP-7 Project under Grant No. 261670.

References

[1] J. Seliger, V. Žagar, R. Blinc, A new highly sensitive ^{1}H–^{14}N nuclear-quadrupole double-resonance technique, J. Magn. Reson. Ser. A 106 (1994) 214–222.
[2] V.S. Grechishkin, N.J. Sinjavsky, New technologies: nuclear quadrupole resonance as an explosive and narcotic detection technique, Phys. – Uspekhi 40 (1997) 393–404.
[3] J. Lužnik, J. Pirnat, V. Jazbinšek, T. Apih, A. Gregorovič, R. Blinc, J. Seliger, Z. Trontelj, Polarization enhanced "single shot" ^{14}N nuclear quadrupole resonance detection of trinitrotoluene at room temperature, Appl. Phys. Lett. 89 (2006) 123509.
[4] R.A. Marino, R.F. Connors, Orthorhombic and monoclinic TNT: a nitrogen ^{14}NQR study, J. Mol. Struct. 111 (1983) 323–328.
[5] T.P. Das, E.L. Hahn, Nuclear Quadrupole Resonance Spectroscopy, Academic Press, New York, 1958.
[6] A. Abragam, The Principles of Nuclear Magnetism, Clarendon, Oxford, 1961.
[7] http://www.spincore.com/products/iSpinNMR/iSpin-NMR.shtml.
[8] N. Sun, T.J. Yoon, H. Lee, W. Andress, R. Weissleder, D. Ham, Palm NMR and 1-Chip NMR, IEEE J. Solid-State Circ. 46 (2011) 342–352.
[9] G. Eidmann, R. Savelsberg, P. Blumler, B. Blümich, The NMR MOUSE, a mobile universal surface explorer, J. Magn. Reson. A 122 (1) (1996) 104–109.
[10] http://www.ettus.com/product/details/UN200-KIT.
[11] D.E. Norton, F.P. Allen, Transistor Amplifier with Impedance Matching Transformer, Patent 3891934, 1975.
[12] http://www.ni.com/labview/.
[13] J. Pirnat, J. Lužnik, V. Jazbinšek, V. Žagar, J. Seliger, Thomas M. Klapötke, Z. Trontelj, ^{14}N NQR in the tetrazole family, Chem. Phys. 364 (2009) 98–104.
[14] A.N. Garroway, M.L. Buess, J.P. Yesinowski, J.B. Miller, Narcotics and explosives detection by ^{14}N pure NQR, Proc. SPIE 2092 (1993) 318–327.
[15] L.V. Myznikov, A. Hrabalek, G.I. Koldobskii, Drugs in the tetrazole series, Chem. Heterocycl. Compd. 43 (2007) 1–9.
[16] S. Harkishan, A.S. Chawla, V.K. Kapoor, D. Paul, R.K. Malhotra, Medicinal chemistry of tetrazoles, Prog. Med. Chem. 17 (1980) 151.
[17] R.J. Herr, 5-Substituted-1H-tetrazoles as carboxylic acid isosteres: medicinal chemistry and synthetic methods, Bioorg. Med. Chem. 10 (2002) 3379–3393.
[18] E.B. Baker, A.I. Popov, Nitrogen-14 nuclear magnetic resonance study of 1,5-disubstituted tetrazoles, J. Phys. Chem. 76 (1972) 2403–2404.
[19] T.M. Klapötke, High energy density materials, Struct. Bond. 125 (2007) 85–121.
[20] T.M. Klapötke, N.K. Minara, J. Stierstorfer, Investigations of bis(methyltetrazolyl)triazenes as nitrogen-rich ingredients in solid rocket propellants – synthesis, characterization and properties, Polyhedron 28 (2009) 13–26.
[21] T.M. Klapötke, M. Sabate, Bistetrazoles: nitrogen-rich, high-performing, insensitive energetic compounds, Chem. Mater. 20 (2008) 3629–3637.
[22] K.F. Khaled, M.M. Al-Quahtani, The inhibitive effect of some tetrazole derivatives towards Al corrosion in acid solution: chemical, electrochemical and theoretical studies, Mater. Chem. Phys. 113 (2009) 150–158.
[23] G.I. Koldabskii, V.A. Ostrovskii, Usp. Khim. 63 (1994) 847–865.
[24] Z. Lavrič, J. Pirnat, J. Lužnik, J. Seliger, V. Žagar, Z. Trontelj, S. Srčič, Application of ^{14}N NQR to the study of piroxicam polymorphism, J. Pharm. Sci. 99 (2010) 4857–4865.
[25] J. Seliger, R. Blinc, H. Arend, R. Kind, Proton-^{14}N double resonance study of the structural phase transitions in the perovskite type layer compound $(CH_3NH_3)_2CdCl_4$, Z. Phys. B 25 (1976) 189–195.
[26] D. Stephenson, J.A.S. Smith, Nitrogen-14 quadrupole cross-relaxation spectroscopy, Proc. Roy. Soc. A 416 (1988) 149–178.
[27] J. Seliger, V. Žagar, Measurement of the ^{14}N nuclear quadrupole resonance frequencies by the solid effect, J. Magn. Reson. 193 (2008) 54–62.
[28] J. Lužnik, J. Pirnat, V. Jazbinšek, Z. Lavrič, S. Srčič, Z. Trontelj, The influence of pressure in paracetamol tablet compaction on ^{14}N nuclear quadrupole resonance signal, Appl. Magn. Reson. 44 (2013) 735–743.
[29] J. Lužnik, J. Pirnat, V. Jazbinšek, Z. Lavrič, T. Apih, R. Blinc, J. Seliger, Z. Trontelj, Improved ^{14}N nuclear quadrupole resonance detection of trinitrotoluene using polarization transfer from protons to ^{14}N nuclei, J. Appl. Phys. 102 (2007) 084903.